



UNIVERSITY OF LEEDS

This is a repository copy of *Laser Photolysis Kinetic Study of OH Radical Reactions with Methyl Tert-Butyl Ether and Trimethyl Orthoformate under Conditions Relevant to Low Temperature Combustion; Measurements of Rate Coefficients and OH Recycling.*

White Rose Research Online URL for this paper:

<https://eprints.whiterose.ac.uk/140190/>

---

**Article:**

Potter, DG [orcid.org/0000-0002-0656-5657](https://orcid.org/0000-0002-0656-5657), Wiseman, S [orcid.org/0000-0002-0269-6684](https://orcid.org/0000-0002-0269-6684), Blitz, MA [orcid.org/0000-0001-6586-7981](https://orcid.org/0000-0001-6586-7981) et al. (1 more author) (2018) Laser Photolysis Kinetic Study of OH Radical Reactions with Methyl Tert-Butyl Ether and Trimethyl Orthoformate under Conditions Relevant to Low Temperature Combustion; Measurements of Rate Coefficients and OH Recycling. *The journal of physical chemistry. A*, 122 (50). pp. 9701-9711. ISSN 1089-5639

<https://doi.org/10.1021/acs.jpca.8b09122>

---

© 2018, ACS. This is an author produced version of a paper published in *The journal of physical chemistry A*. Uploaded in accordance with the publisher's self-archiving policy.

**Reuse**

Items deposited in White Rose Research Online are protected by copyright, with all rights reserved unless indicated otherwise. They may be downloaded and/or printed for private study, or other acts as permitted by national copyright laws. The publisher or other rights holders may allow further reproduction and re-use of the full text version. This is indicated by the licence information on the White Rose Research Online record for the item.

**Takedown**

If you consider content in White Rose Research Online to be in breach of UK law, please notify us by emailing [eprints@whiterose.ac.uk](mailto:eprints@whiterose.ac.uk) including the URL of the record and the reason for the withdrawal request.



[eprints@whiterose.ac.uk](mailto:eprints@whiterose.ac.uk)  
<https://eprints.whiterose.ac.uk/>

# Laser Photolysis Kinetic Study of OH Radical Reactions with Methyl tert-Butyl Ether and Trimethyl Orthoformate under Conditions Relevant to Low Temperature Combustion; Measurements of Rate Coefficients and OH Recycling

David G. Potter<sup>1,2</sup>, Scott Wiseman<sup>1</sup>, Mark A. Blitz<sup>1,3</sup> and Paul W. Seakins<sup>\*1,3</sup>

<sup>1</sup>*School of Chemistry, University of Leeds, Leeds, LS2 9JT, UK*

<sup>2</sup>*School of Chemical and Process Engineering, University of Leeds, Leeds, LS2 9JT, UK*

<sup>3</sup>*National Centre for Atmospheric Science, University of Leeds, Leeds, LS2 9JT, UK*

## Abstract

Methyl tertiary butyl ether (MTBE) and trimethyl orthoformate (TMOF) are potential biofuel ethers, and could replace conventional fossil fuels, or act as additives to aid combustion. Laser flash photolysis with laser-induced fluorescence detection of the OH radical has been used to measure the rate coefficients of the OH reaction with these ethers, from 298 K to approximately 740 K. The temperature dependence of the rate coefficients is parameterised as:

$$k_{\text{OH}+\text{MTBE}}(298\text{--}680\text{ K}) = 9.8 \times 10^{-13} \left(\frac{T}{298}\right)^{2.7} \times \exp\left[\frac{2500}{RT}\right] \text{ cm}^3 \text{ molecule}^{-1} \text{ s}^{-1}$$
$$k_{\text{OH}+\text{TMOF}}(298\text{--}744\text{ K}) = 8.0 \times 10^{-13} \left[ \left(\frac{T}{298}\right)^{2.6} + \left(\frac{T}{298}\right)^{-8.1} \right] \times \exp\left[\frac{2650}{RT}\right] \text{ cm}^3 \text{ molecule}^{-1} \text{ s}^{-1}$$

The room temperature (298 K) bimolecular rate coefficients were measured as  $k_{\text{OH}+\text{MTBE}} = (2.81 \pm 0.32) \times 10^{-12} \text{ cm}^3 \text{ molecule}^{-1} \text{ s}^{-1}$  and  $k_{\text{OH}+\text{TMOF}} = (4.65 \pm 0.50) \times 10^{-12} \text{ cm}^3 \text{ molecule}^{-1} \text{ s}^{-1}$  where the errors represent statistical uncertainties at the  $2\sigma$  level in combination with an estimated 10% systematic error. Regeneration of OH radicals was observed for both reactions at higher temperatures in the presence of  $\text{O}_2$  via biexponential OH decays, which were observed above 489 K, and 568 K, for TMOF and MTBE respectively. The OH yield from MTBE/ $\text{O}_2$  between 620 and 700 K, was invariant with the concentration of oxygen ( $10^{15} - 10^{18} \text{ molecule cm}^{-3}$ ) at  $(36 \pm 5) \%$ . Mechanisms for OH regeneration from MTBE are briefly discussed and compared with those in the literature and from dimethyl and diethyl ether. The lower OH yield from MTBE, compared to these other ethers, is most likely due to competition with an  $\text{HO}_2$  formation channel.

## Introduction

Biofuel alternatives to conventional fossil fuels can significantly lower carbon emissions from combustion, but in 2016 only accounted for 4 % of global road transport energy consumption.<sup>1</sup> Dimethyl ether (DME) and oxymethylene ether (OME) (Figure 1) have already been the subject of considerable academic<sup>2-7</sup> and industrial research,<sup>8-9</sup> showing promise in reducing

emissions and increasing fuel efficiency.<sup>8, 10</sup> For biofuels to be used in novel engines, such as the homogeneous charge compression ignition (HCCI) engine, an understanding of the mechanism by which they autoignite is required.<sup>11</sup> Autoignition relies on chain-branching of radicals, and despite several studies, particularly on methyl tertiary butyl ether (MTBE),<sup>12-22</sup> the chemical mechanism for chain-branching, has not yet been verified for the biofuel ethers discussed in this work.

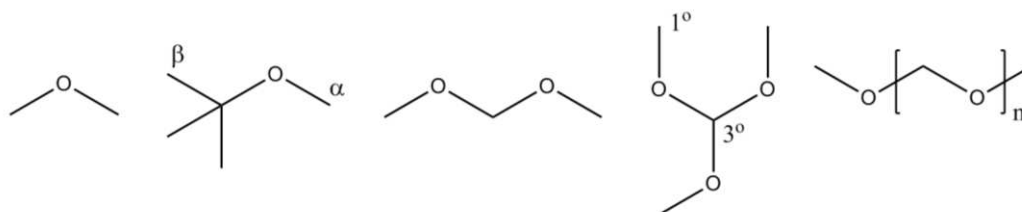
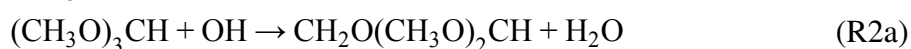
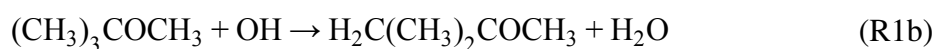


**Figure 1.** Molecular structures for DME, MTBE, dimethoxy methane (DMM), TMOF and OME (left to right). Alpha and beta sites are labelled for MTBE, and the locations of the primary and tertiary hydrogens are labelled for TMOF.

MTBE and trimethyl orthoformate (TMOF) both bear structural similarities to DME (Figure 1), and can be synthesised using methanol (and therefore bio-methanol).<sup>23-24</sup> MTBE has been used as an additive to improve the octane rating of fuels,<sup>10</sup> and TMOF has been investigated for its use in fuel cells.<sup>25-26</sup> Few studies exist on the low temperature oxidation mechanism of either ether. For simple hydrocarbon fuels, the preliminary reactions for their low temperature combustion are well-documented,<sup>27</sup> with the initial propagation step consisting of hydrogen atom abstraction by a small radical. OH is generally the most important species under low temperature combustion conditions due to its fast reaction with hydrocarbons. MTBE and TMOF both possess two distinct sites that the hydroxyl radical can abstract from;  $\alpha$  (R1a) and  $\beta$  (R1b) primary sites for MTBE; primary (R2a) and tertiary (R2b)  $\alpha$  sites for TMOF. The products of these reactions are H<sub>2</sub>O and a radical, R. This first step has been measured in this work, with a non-site-specific approach, thus reported values for  $k_1$  and  $k_2$  refer to the sum of the rate coefficients for reactions 1a and 1b, and reactions 2a and 2b, respectively.



After the initial abstraction step, all of the R radical products above (reactions 1a – 2b) are expected to follow the general mechanism shown below (Figure 2), where addition of molecular oxygen to the R radical leads to formation of an RO<sub>2</sub> radical. Decomposition of the R radical is in competition with the oxygen addition reaction.

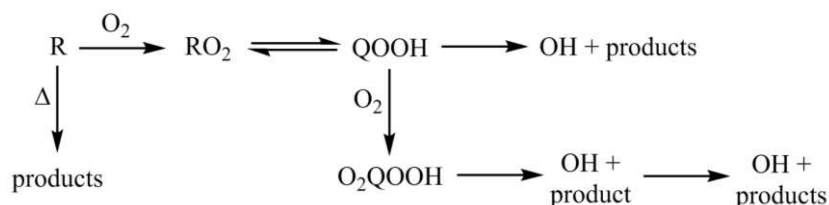


**Figure 2.** Mechanism for low temperature chain-branching of fuels.<sup>28-29</sup>

Internal rearrangement of RO<sub>2</sub>, *via* an internal hydrogen abstraction, can then take place producing a QOOH radical.<sup>30</sup> RO<sub>2</sub> to QOOH rearrangement can occur at different sites. Radical propagation by formation of an OH radical can occur by decomposition of the QOOH radical to various products. Alternatively, with sufficient oxygen, low temperature oxidation of the ether-derived radicals can progress *via* a second oxygen addition, forming a peroxy radical (O<sub>2</sub>QOOH). This radical can decompose to a peroxy formate product, and the first OH radical of chain-branching. The peroxy formate product decomposes again to form additional radical products. Low temperature autoignition is suggested to occur by this chain-branching process.<sup>29, 31-32</sup>

No isolated measurements have been made concerning the later steps of these combustion mechanisms for MTBE, and previous research has not covered  $k_1$  comprehensively, with few extensive temperature dependent studies conducted, and no OH recycling measurements. A full summary of past work on  $k_1$  is presented in Table 2 in the Results section. Only two studies have been undertaken across large temperature ranges comparable to our measurements.<sup>12, 14</sup> All other studies were carried out at 440 K and below. There has been some discussion in the literature of the two possible MTBE sites for hydrogen abstraction, but no direct experimental measurements of the site-specific rate coefficients. Arif et al.<sup>12</sup> predicted ~80 % and ~20 % abstraction from the  $\alpha$  and  $\beta$  sites respectively, based on previous product analysis from smog chamber experiments.<sup>33-34</sup> The dominance of abstraction from the methyl site rather than the t-butyl site was expected due to the weaker C-H bonds on the  $\alpha$  carbon. Theoretical studies by Iuga et al.<sup>35</sup>, Zavala-Oseguera et al.<sup>36</sup> and Atadinc et al.<sup>37</sup> have all indicated similar branching ratios for H abstraction (~75 %, 74 % and 63 % abstraction

from the  $\alpha$  site respectively). In this work, the OH removal kinetics of MTBE are reported as a total of both possible reaction routes, and the OH yields are measured as a weighted average of both R radical routes, where one may contribute more than the other, but experiments here do not differentiate between the two sites. Mechanistic discussion of the OH recycling process is generally limited to the major abstraction site, but both routes are similar.

Trimethyl orthoformate and hydroxyl radical kinetics have only been studied once, by Platz et al.<sup>38</sup> using pulse radiolysis and UV absorption, finding  $k_2 = (6.0 \pm 0.5) \times 10^{-12} \text{ cm}^3 \text{ molecule}^{-1} \text{ s}^{-1}$  at 295 K, which they compared to OH + DMM (dimethoxymethane, Figure 1), a similarly structured molecule, where  $k_{\text{OH+DMM}} = 5.2 \times 10^{-12} \text{ cm}^3 \text{ molecule}^{-1} \text{ s}^{-1}$  as an average of two measurements.<sup>39-40</sup> No measurements were made above room temperature.

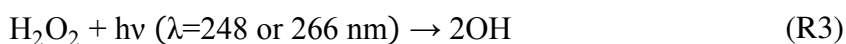
This paper presents a temperature-dependent study of OH + MTBE, the first temperature-dependent study of OH + TMOF rate coefficients, and analysis of biexponential behaviour that was observed for MTBE, with suggestions of the mechanism that gives rise to the OH yields measured.

## Experimental

Conventional slow flow laser flash photolysis was combined with laser-induced fluorescence to monitor OH.<sup>41-42</sup> The reactants (MTBE or TMOF) (99 % and 99.8 %, both Sigma-Aldrich) ([MTBE] range used =  $(1.6 - 11.6) \times 10^{14} \text{ molecule cm}^{-3}$ , [TMOF] range used =  $(0.3 - 7.9) \times 10^{14} \text{ molecule cm}^{-3}$ ), OH precursor (hydrogen peroxide,  $\text{H}_2\text{O}_2$ ) (Sigma-Aldrich, 50 % (w/w) in  $\text{H}_2\text{O}$ ), buffer gas ( $\text{N}_2$ ) (BOC), and  $\text{O}_2$  (BOC) (approximate  $[\text{O}_2]$  range used =  $10^{14} - 10^{18} \text{ molecule cm}^{-3}$ ) were flowed through calibrated mass flow controllers (MFCs) into a mixing manifold and through the stainless steel reaction cell. Generally experiments in this work were carried out at an approximate flow rate of  $1 \text{ L min}^{-1}$  and 60 Torr of pressure, or  $2 \text{ L min}^{-1}$  and 120 Torr, except for chemical activation experiments which were carried out at  $1 \text{ L min}^{-1}$  and 10 Torr pressure. For experiments carried out above room temperature, the reaction cell was heated using cartridge heaters. A calibrated K-type thermocouple was used to measure the temperature close to the entrance of the cell. A capacitance manometer (MKS Baratron, 0 – 1000 Torr) was used to measure the pressure inside the reaction cell, and throttling of the rotary pump (Edwards RV 5) by a needle valve was used to control the pressure.

Hydrogen peroxide was delivered with N<sub>2</sub> using a bubbler placed before a MFC, to ensure the amount of gas being delivered was known. Approximately 0.5 L min<sup>-1</sup> needed to be flowed before reasonable OH signal was seen, which suggests a significant fraction of hydrogen peroxide was lost in the MFC. Contact of hydrogen peroxide with the metal in the MFC and consequent decomposition results in some oxygen always being delivered to the system, which was estimated to be approximately 10<sup>15</sup> molecule cm<sup>-3</sup>, but this varied depending on pressure and flow. Under typical conditions of 298 K, 30 Torr, 1 L min<sup>-1</sup> flow, the estimated amount of H<sub>2</sub>O (from the hydrogen peroxide precursor) delivered was approximately 1.5 % of the total gas density (~10<sup>18</sup> molecule cm<sup>-3</sup>), and thus we expect H<sub>2</sub>O to make a negligible contribution, acting as a buffer gas.

Photolysis of hydrogen peroxide was used to generate the hydroxyl radicals, and was the source of OH for all experiments in this work:



The H<sub>2</sub>O<sub>2</sub> precursor was photolysed using an excimer laser operating at 248 nm (KrF, Lambda Physik LPX 200, 10 Hz pulse repetition frequency, typical energy 40 – 80 mJ pulse<sup>-1</sup> cm<sup>-2</sup>, beam dimensions 25 mm × 10 mm), with some experiments using a 266 nm pulsed Nd:YAG laser (Q-smart 850 by Quantel, 10 Hz pulse repetition frequency, 9 mm beam diameter) for photolysis. The photon density was approximately 7.5 × 10<sup>16</sup> photons cm<sup>-2</sup>, and the typical OH concentration was ~1 × 10<sup>12</sup> molecule cm<sup>-3</sup>. On-resonance laser-induced fluorescence was used, probing the OH radicals at ~308 nm, corresponding to the energy of the OH Q<sub>1</sub>(2) rotational line of the A<sup>2</sup>Σ(v' = 0) ← X<sup>2</sup>Π(v'' = 0) transition. The probe laser light was obtained from the output of an Nd:YAG-pumped (Continuum Precision II, 532 nm) dye laser (Sirah PRSC-DA-24, 10 Hz, energy <0.1 mJ pulse<sup>-1</sup>, 3 mm beam diameter, DCM Special dye). The dye laser output at ~616 nm was doubled to output ~308 nm light for OH detection. Fluorescence from the OH radicals at ~308 nm was detected by a photomultiplier (Electron Tubes), after passing through a filter ((308 ± 5) nm, Barr Associates). A digital oscilloscope (LeCroy LT 372) integrated the fluorescence signal, before transferring the output to the personal computer for collection and analysis, where the fluorescence signal was normalised for probe laser power.

To build up a time-dependent trace of OH fluorescence signal, the delay time between the photolysis and probe lasers was varied using a delay generator, with a typical decay trace

consisting 220 points, each averaged 3 – 8 times. The total gas flow ensured each laser shot photolysed a fresh sample of gas, and varying the photolysis laser energy by a factor of three was shown not to affect the kinetic traces obtained. Probing on-resonance necessitated the use of temporal gating (~30 ns) to avoid detecting the scatter pulse from the probe laser. A typical OH decay for the reaction of OH with MTBE is shown in the inset to Figure 3.

Reactions were studied under pseudo-first order conditions where [ether]  $\gg$  [OH]. The resulting single exponential decays were fit to Equation 1 using a nonlinear least-squares method. OH + ether removal experiments were conducted over the ranges 298 – 744 K, and 29 – 68 Torr.

$$I_{f,t} = I_{f,0}e^{-k't} \quad (\text{E1})$$

Here,  $I_f$  is the intensity of the OH fluorescence (proportional to [OH]),  $k' = k_d + ([\text{ether}] \times k_1 \text{ or } k_2)$ . The bimolecular rate coefficients were obtained from the slope of the plot of the phenomenological rate constant  $k'$  versus [ether], where the intercept,  $k_d$ , was the rate coefficient for loss of OH in the absence of ether, primarily from the OH + H<sub>2</sub>O<sub>2</sub> reaction. An example bimolecular plot is shown in Figure 3 and the returned bimolecular rate coefficients are presented in Table 1.

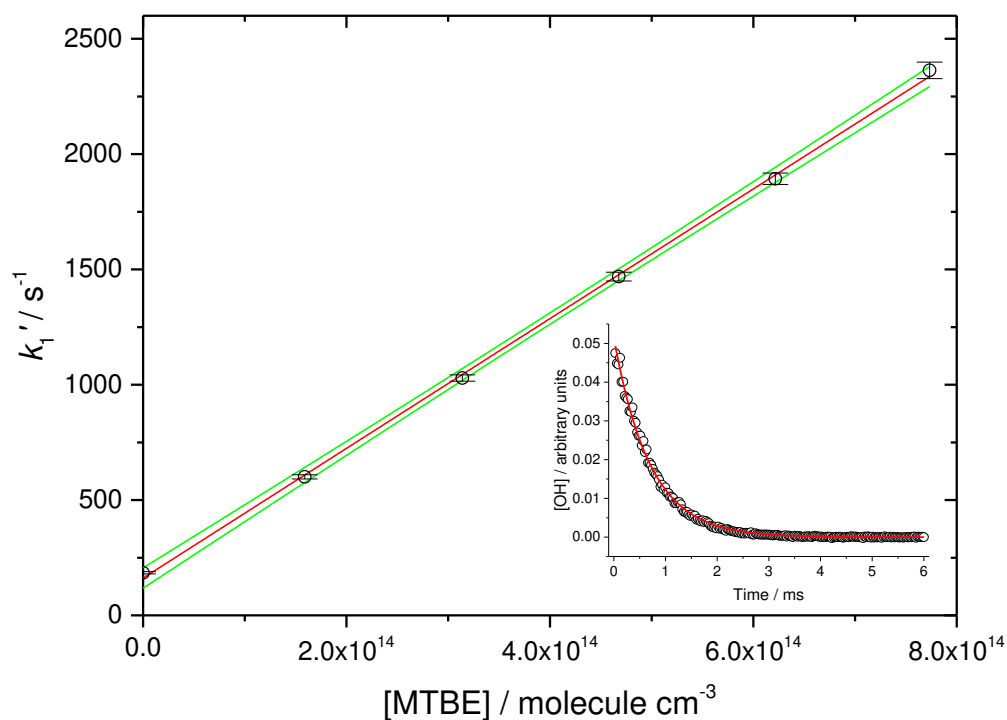


**Figure 3.** Example bimolecular plot for OH + MTBE at 298 K, 29 Torr,  $k_1 = (2.81 \pm 0.18) \times 10^{-12} \text{ cm}^3 \text{ molecule}^{-1} \text{ s}^{-1}$ . The inset shows an example single exponential decay,  $[\text{MTBE}] = 4.7 \times 10^{14} \text{ molecule cm}^{-3}$ . An exponential fit yielded  $k_1' = (1470 \pm 20) \text{ s}^{-1}$ . Green lines are 95 % confidence limits, and error bars are statistical at the  $2\sigma$  level. Uncertainties on returned parameters are statistical at the  $2\sigma$  level.

Kinetic traces measured at higher temperatures (above 568 K for MTBE and 489 K for TMOF) in the presence of  $\text{O}_2$  are biexponential decays (an example of which is shown in Figure 5), rather than a single exponential decay. The initial fast decay in the biexponential traces is the reaction between OH and the ether ( $k_a'$ ), and the second, tail portion of the decay, contains information about the regeneration of OH ( $k_b$  and  $k_c$ ) (thus the decay is slower in the tail). These more complex traces were analysed by fitting to an equation derived from the scheme shown in Figure 4.

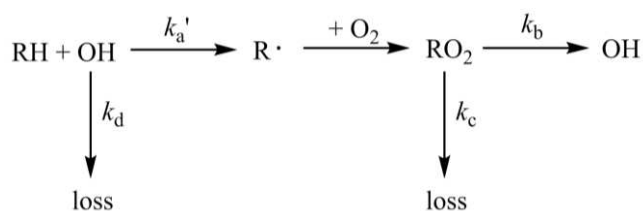


**Figure 4.** Simplified reaction scheme for biexponential analysis equation parameters.

This differs from the scheme in Figure 2 in that the O<sub>2</sub>QOOH species is not considered; rather, OH formation only arises from RO<sub>2</sub> (via decomposition of QOOH). The OH traces were fitted with the following equation:

$$[\text{OH}] = [\text{OH}]_0 \times \left[ \left( \frac{-(k_d + k_a') - L_2}{L_1 - L_2} \right) \times (e^{L_1 \times t} - e^{L_2 \times t}) + e^{L_2 \times t} \right] \quad \text{E2}$$

Here,  $k_a'$  = pseudo first-order rate coefficient for reaction 1a+1b, or 2a+2b,  $k_d$  = rate coefficient for OH loss in the absence of ether, and the terms  $L_1$  and  $L_2$  are expanded fully in Equations S1 – S4 in the Supporting Information. The terms  $k_b$  (first order rate coefficient for OH regeneration from the R radical) and  $k_c$  (first order rate coefficient for R radical reacting without producing OH) are both present in the  $L_1$  and  $L_2$  terms. This equation can be used to determine the parameters from single trace analysis, where parameters are best defined when [ether] is sufficiently high that  $k_a'$  is faster than the sum of  $k_c$  and  $k_b$ . Parameters are even better defined/more robust when using global analysis, as the information is taken from many traces; global analysis was used in this paper.

For robust parameter retrieval, global fitting was used to analyse several biexponential traces at once ( $k_a' = k_{1,2}[\text{ether}]$  for each trace), and share the bimolecular rate coefficient between decays. In this process the initial signal intensity,  $k_a'$ ,  $k_b$  and  $k_c$  are local parameters for each trace and rate coefficient  $k_{1,2}$  is shared globally across all traces in the fit. This allows a well-defined, robust bimolecular rate coefficient for each temperature to be obtained from kinetic traces, which contain information on  $k_a'$  in the earlier part of the trace. The bimolecular rate coefficients  $k_1$  and  $k_2$  obtained are listed in Table 1.

**TABLE 1:** Obtained bimolecular rate coefficients for  $k_1$  and  $k_2$ . Uncertainties are  $2\sigma$  with an additional 10 % of the measurement value added to account for systematic errors.

OH + MTBE (R1)			OH + TMOF (R2)		
$T / \text{K}$	$10^{12} k_1 / \text{cm}^3 \text{ molecule}^{-1} \text{ s}^{-1}$	$P / \text{Torr}$	$T / \text{K}$	$10^{12} k_2 / \text{cm}^3 \text{ molecule}^{-1} \text{ s}^{-1}$	$P / \text{Torr}$
298	$2.81 \pm 0.37^a$	29	298	$4.69 \pm 0.83$	37
298	$2.80 \pm 0.53^a$	39	298	$4.73 \pm 0.84$	68
354	$3.00 \pm 0.70$	37	298	$4.53 \pm 0.92$	61
395	$4.18 \pm 0.76$	37	336	$3.34 \pm 0.49$	68
441	$6.15 \pm 1.19$	37	338	$3.75 \pm 0.56$	61
495	$7.27 \pm 1.68^a$	63	380	$4.65 \pm 0.98$	64
510	$8.43 \pm 1.45$	45	451	$5.26 \pm 0.70$	37
568	$10.6 \pm 1.2^b$	52	489	$5.71 \pm 0.67^b$	64
604	$10.4 \pm 1.2^{ab}$	62	540	$7.05 \pm 0.82^b$	61
605	$10.8 \pm 1.2^b$	45	598	$7.75 \pm 0.97^b$	60
624	$11.2 \pm 1.3^b$	38	642	$9.88 \pm 1.14^b$	61
646	$12.6 \pm 1.5^b$	45	675	$10.5 \pm 1.2^b$	60
653	$13.5 \pm 1.6^b$	67	704	$11.9 \pm 1.3^b$	60
680	$14.4 \pm 1.7^b$	45	734	$14.0 \pm 1.7^b$	59
707	$13.1 \pm 2.1^b$	46	744	$14.7 \pm 1.9^b$	62
727	$12.4 \pm 1.6^b$	46			

<sup>a</sup> Experiments using 266 nm photolysis laser. All others were 248 nm.

<sup>b</sup> From global analysis.

## Results and Discussion

**Kinetics of OH + MTBE.** Rate coefficients for the abstraction of hydrogen by OH from methyl tert-butyl ether ( $k_1$ ) were measured as a function of temperature, using hydrogen peroxide as a photolytic precursor, in the ranges 298 – 727 K and 29 – 67 Torr. The measured rate coefficients did not vary significantly with laser power or laser repetition rate (5.9 % maximum variation between 10, 5 and 2 Hz, and no variation within uncertainties). Additionally, varying the photolysis wavelength between 248 and 266 nm produced no significant variation in the bimolecular rate coefficient. Although there are no reported UV cross sections for MTBE, this lack of variation with photolysis wavelength is consistent with the insignificant cross-sections for smaller ethers at 248 nm and 266 nm.<sup>43</sup>

At temperatures greater or equal to 568 K, the OH signal could no longer be represented as a single exponential, rather, the OH signal decay was biexponential. The presence of some

oxygen when delivering hydrogen peroxide by a mass flow controller, allowed OH regeneration to occur *via* the scheme shown in Figure 4.

Figure 5 demonstrates the poor fit of a single exponential decay equation to the data obtained at 568 K and above, and the good fit by the biexponential equation.

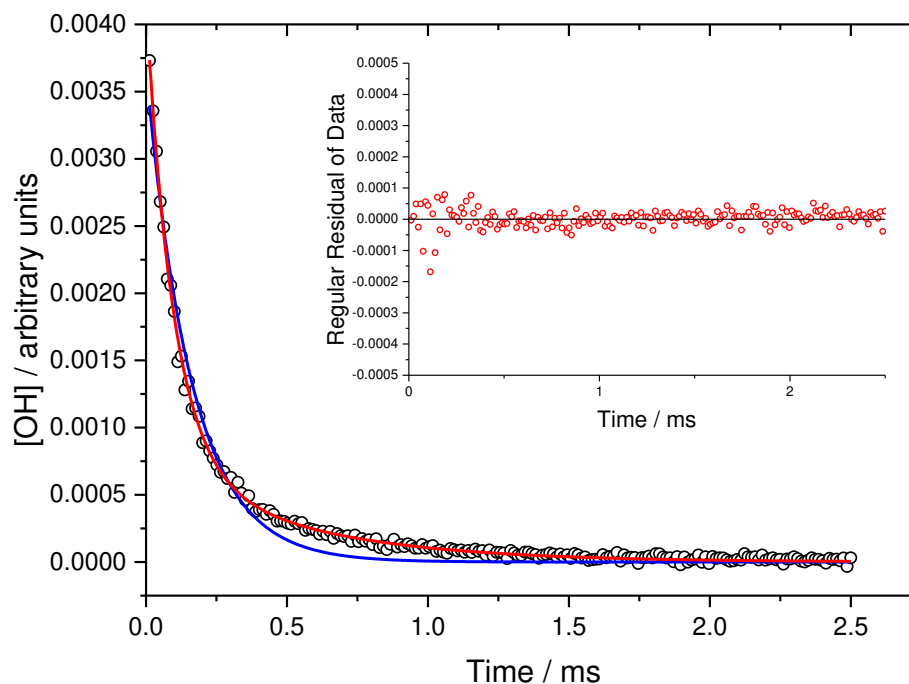


**Figure 5.** Example OH + MTBE biexponential decay with a good fit to the biexponential equation (red line), and a poor fit to the single exponential equation (blue line), measured at 680 K, 45 Torr. The inset shows the residuals for the biexponential fit. The initial fast portion of the decay contains information on  $k_a'$ , whereas  $k_b$  and  $k_c$  are contained in the tail of the trace. Parameters from the biexponential fit:  $k_a' = (8710 \pm 250) \text{ s}^{-1}$ ,  $k_b = (1270 \pm 140) \text{ s}^{-1}$ ,  $k_c = (2330 \pm 200) \text{ s}^{-1}$ , and  $k_d$  was fixed at  $200 \text{ s}^{-1}$ . Parameters from the single exponential fit:  $k_1' = (6210 \pm 260) \text{ s}^{-1}$ .  $[\text{MTBE}] = 6.09 \times 10^{14} \text{ cm}^3 \text{ molecule}^{-1} \text{ s}^{-1}$ . Uncertainties are statistical at the  $2\sigma$  level.

The Arrhenius plot for  $k_1$  is shown in Figure 6 and  $k_1(T)$  can be described by  $k_1(298\text{--}680 \text{ K}) = 9.8 \times 10^{-13} \left(\frac{T}{298}\right)^{2.7} \times \exp\left[\frac{2500}{RT}\right] \text{ cm}^3 \text{ molecule}^{-1} \text{ s}^{-1}$ . Across the temperature range relevant to this work (298 – 680 K), the uncertainty of the Arrhenius parameterisation is 12.7 % – the maximum size of the 95 % confidence limits. A weighted fit was used to describe the temperature dependency of the data obtained, and the highest two temperature measurements

were omitted, as a result of the apparent decrease in rate coefficient, which was attributed to decomposition of the MTBE at high temperatures.

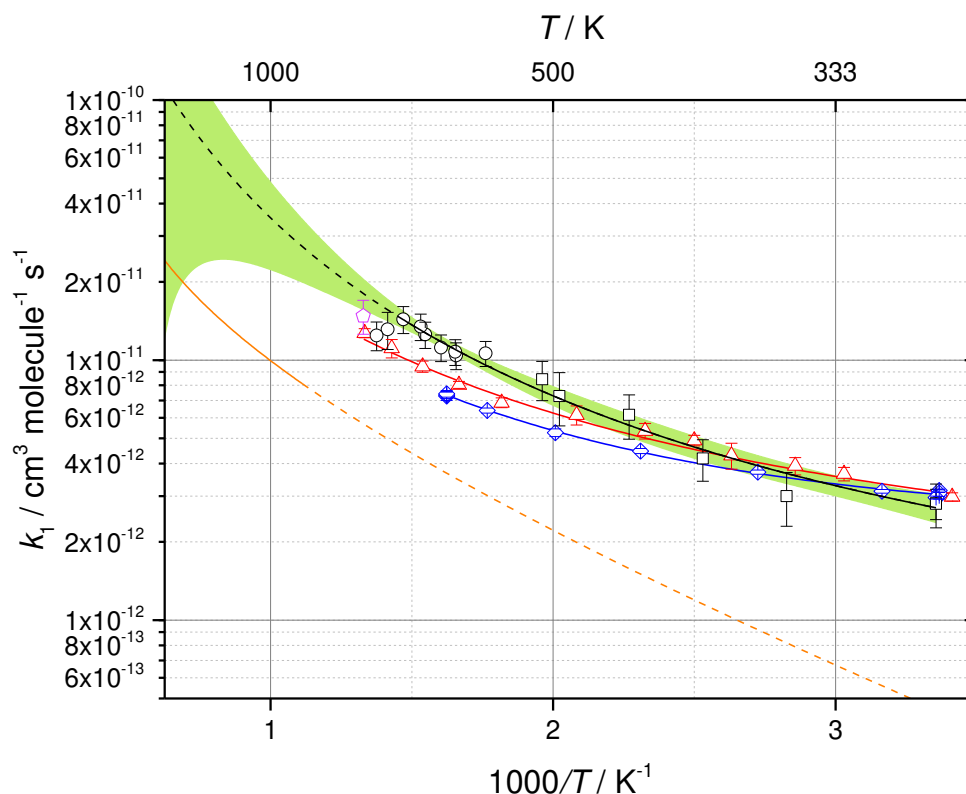


**Figure 6.**  $k_1$  measured in this work (black), as a function of temperature, with a modified Arrhenius fit (excluding the highest two temperatures):  $k_1(298\text{--}680\text{ K}) = 9.8 \times 10^{-13} \left(\frac{T}{298}\right)^{2.7} \times \exp\left[\frac{2500}{RT}\right]$   $\text{cm}^3 \text{ molecule}^{-1} \text{ s}^{-1}$ , where the 95 % confidence bounds are shown in green shading. The black dashed line shows the Arrhenius parameterisation extrapolated past the experimental conditions of this work. Single exponential (black squares) and biexponential data (black circles) are indicated. Uncertainties are  $2\sigma$  with an additional 10 % of the value to account for systematic errors. Literature measurements, and their modified Arrhenius fits, are shown for Arif et al.<sup>12</sup> (red triangles), Bonard et al.<sup>14</sup> (blue diamonds) and Tranter and Walker (magenta pentagon).<sup>44</sup> The modelled modified Arrhenius expression used by Yasunaga et al.<sup>45</sup> is shown for their validated temperature range (orange) and extrapolated to lower temperatures (orange dashed).

Below approximately 400 K, the values of  $k_1$  from this work overlap with the measurements of Arif et al.<sup>12</sup> and Bonard et al.<sup>14</sup>, however above this temperature higher rate coefficients were measured. Biexponential decays were not observed prior to this work, despite Bonard et al. using  $\text{H}_2\text{O}_2$  as their OH precursor, meaning their experiment potentially contained

oxygen. The small number of data points (~8 per trace), may have been insufficient to reveal biexponential behaviour. Any unaccounted biexponential behaviour would have resulted in extraction of their pseudo-first order rate coefficients lower than the actual values. An example of the lower value of  $k_1'$  extracted from a single exponential fit to biexponential data can be seen in the reported  $k_1'$  and  $k_a'$  values in Figure 5.

Measurements made by Arif et al.<sup>12</sup> were made using photodissociation of N<sub>2</sub>O at 193 nm, and subsequent reaction of O(<sup>1</sup>D) with H<sub>2</sub>O to generate OH radicals. Lower rate coefficients measured by Arif et al. in comparison with this work may be as a result of photolysis of their reactant at the lower wavelength used, or relaxation of excited OH radicals over the duration of a kinetic decay. Based on the absorption cross-section of diethyl ether, at room temperature, a reasonable estimate of MTBE's cross-section at 193 nm would be approximately 10<sup>-18</sup> cm<sup>2</sup> molecule<sup>-1</sup>,<sup>43</sup> rather than the estimate of 10<sup>-21</sup> cm<sup>2</sup> molecule<sup>-1</sup> used by Arif et al. There may therefore have been radical-radical reactions which could have affected the OH kinetics. However, Arif et al. reported no variation in rate coefficients as the photolysis laser intensity was changed, suggesting that such effects were not present.

A value of  $k_1 = (1.48 \pm 0.22) \times 10^{-11}$  cm<sup>3</sup> molecule<sup>-1</sup> s<sup>-1</sup> at 753 K was determined by Tranter and Walker<sup>44</sup> using relative rate methods. This value is in good agreement with the current work.

Included in Figure 6 is the modified Arrhenius expression for OH + MTBE hydrogen abstraction employed by Yasunaga et al.<sup>45</sup> to validate data on MTBE oxidation from their shock tube measurements. To our knowledge, these are the only data on reaction 1 above ~750 K. Yasunaga et al. used group additivity rate coefficient estimates based on H abstraction from other molecules, such as DME, ethyl methyl ether, iso-propyl methyl ether, and methyl cyclohexane. Although this expression was only used to validate experiments over the range 900 – 1600 K, when it is extrapolated back only over a relatively short temperature range to the highest temperatures of this work and Arif et al., the extrapolated values are approximately a factor 2 lower (Figure 6). Yasunaga et al. report that unimolecular decomposition reactions of MTBE dominate the chemistry and hence an underestimation of  $k_1$  will have a limited effect on their model:measurement comparison.

The mean room temperature value for the bimolecular rate coefficient for R1 measured in this work is shown in Table 2, along with a summary of literature measurements and their room temperature measurements. The uncertainty in the room temperature rate coefficient from this work is 2 $\sigma$  with an extra 10 % of the measured rate coefficient propagated, to allow for the

systematic errors associated with the experimental method. Our value for  $k_1$  ( $(2.81 \pm 0.32) \times 10^{-12} \text{ cm}^3 \text{ molecule}^{-1} \text{ s}^{-1}$ ) is in good agreement with previous measurements. Considering only the statistical uncertainty ( $\pm 0.12$  at the  $2\sigma$  level), we measured a slightly lower rate than the majority of the literature values, but are in agreement (within errors) with measurements made by Arif et al.<sup>12</sup>, Picquet et al.<sup>18</sup>, Teton et al.<sup>20</sup> and Smith et al.<sup>19</sup>

**TABLE 2:** Comparison of the obtained rate coefficient for  $k_1$  with previous measurements

Reference	Technique	$k_1(298 \text{ K})^a$	$T / \text{K}$	$k(T)^b$
Bonard et al. <sup>14</sup> (2002)	PLP-LIF	$3.05 \pm 0.03^c$	297 – 616	$5.7 \times 10^{-13} (T/298)^{2.4} e^{4.15/RT}$
Picquet et al. <sup>18</sup> (1998)	Relative rate	$2.98 \pm 0.06$	298	–
Arif et al. <sup>12</sup> (1997)	LP-LIF	$2.98 \pm 0.11^d$	293 – 750	$1.3 \times 10^{-12} (T/298)^{2.0} e^{2.21/RT}$
Teton et al. <sup>20</sup> (1996)	PLP-LIF	$3.13 \pm 0.36$	230 – 371	$5.0 \times 10^{-12} \times e^{-1.1/RT}$
Smith et al. <sup>19</sup> (1991)	Relative rate	$2.99 \pm 0.12$	298	–
Bennett and Kerr <sup>13</sup> (1990)	Relative rate	2.84	242-328	$4.0 \times 10^{-12} \times e^{-0.85/RT}$
Wallington et al. <sup>21</sup> (1989)	Relative rate	$3.24 \pm 0.08^e$	295	–
Wallington et al. <sup>22</sup> (1988)	UV photolysis-microwave OH resonance	$3.09 \pm 0.15$	240-440	$5.1 \times 10^{-12} \times e^{-1.29/RT}$
Tranter and Walker <sup>44</sup> (2001)	Relative Rate	na	753	$(1.48 \pm 0.22) \times 10^{-11}$
This work	PLP-LIF	$2.81 \pm 0.32$	298 - 727	$9.8 \times 10^{-13} (T/298)^{2.7} e^{2.5/RT}$

<sup>a</sup> Units are  $10^{-12} \text{ cm}^3 \text{ molecule}^{-1} \text{ s}^{-1}$ .

<sup>b</sup> Units of  $A$  are  $\text{cm}^3 \text{ molecule}^{-1} \text{ s}^{-1}$  and  $E_a$  are  $\text{kJ mol}^{-1}$ .

<sup>c</sup> Measured at 297 K.

<sup>d</sup> Measured at 293 K.

<sup>e</sup> Measured at 295 K.

**Kinetics of OH + TMOF.** Rate coefficients for the abstraction of hydrogen by OH, from trimethyl orthoformate ( $k_2$ ), were measured as a function of temperature using hydrogen peroxide as the OH photolytic precursor, in the ranges 298 – 744 K and 37 – 68 Torr. The reaction of OH with TMOF showed similar behaviour to that with MTBE, in that low temperature OH decays were single exponential, and higher temperature decays were biexponential. However, the OH + TMOF reaction exhibited biexponential behaviour at a lower temperature, where the nature of the decays changed at  $\sim 489$  K. Example decays and a bimolecular plot for TMOF are included in the Supporting Information (Figure S1 and Figure

S2). Measured rate coefficients did not vary significantly with laser power or laser repetition rate (7.0 % maximum variation between 10, 5 and 2 Hz, and no variation within uncertainties).

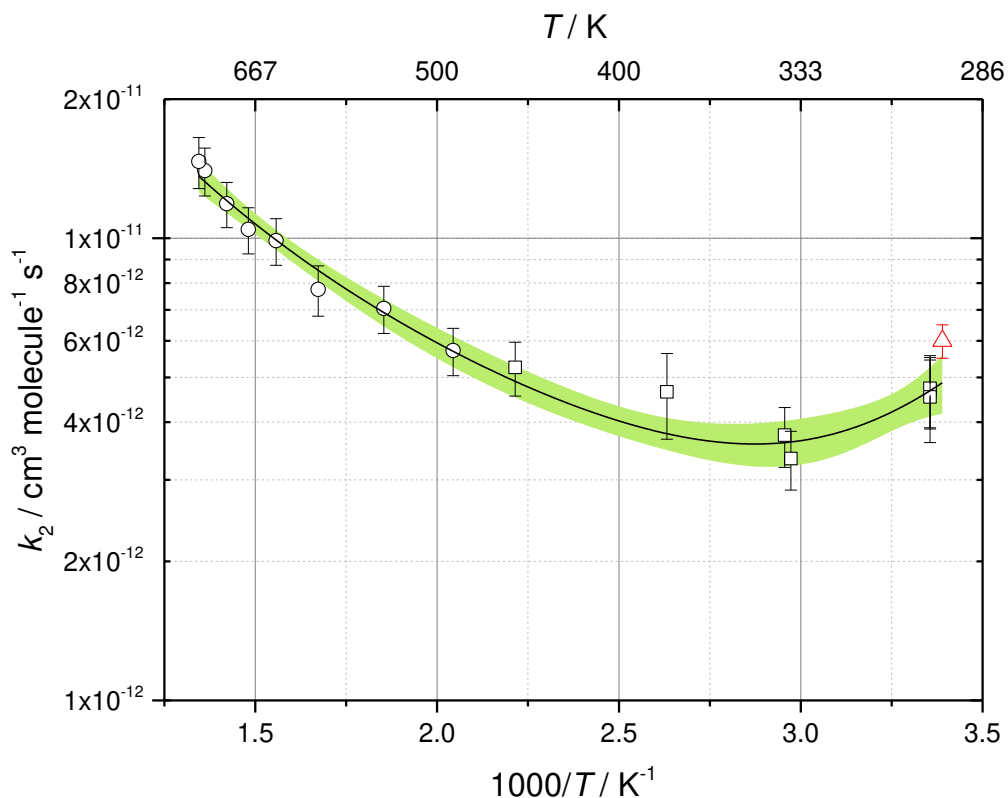


**Figure 7.**  $k_2$  measured in this work (black), as a function of temperature. Single exponential (black squares) and biexponential regions (black circles) are indicated. Errors are  $2\sigma$  with an additional 10 % of the value to account for systematic errors. The only available literature measurement, by Platz et al.<sup>38</sup>, is included (red triangle). The temperature dependency of  $k_2$  from this work can be described by  $k_2(298\text{--}744\text{ K}) = 8.0 \times 10^{-13} \left[ \left( \frac{T}{298} \right)^{2.6} + \left( \frac{T}{298} \right)^{-8.1} \right] \times \exp \left[ \frac{2650}{RT} \right] \text{ cm}^3 \text{ molecule}^{-1} \text{ s}^{-1}$ , where the 95 % confidence bounds are shown in green shading.

Examining the temperature dependence of the bimolecular rate coefficient for the OH + TMOF reaction (Figure 7), there is a clear positive temperature dependence above approximately 340 K, and a small negative temperature dependence region below this temperature. The temperature dependence of the data can be parameterised by  $k_2(298\text{--}744\text{ K}) = 8.0 \times 10^{-13} \left[ \left( \frac{T}{298} \right)^{2.6} + \left( \frac{T}{298} \right)^{-8.1} \right] \times \exp \left[ \frac{2650}{RT} \right] \text{ cm}^3 \text{ molecule}^{-1} \text{ s}^{-1}$ , where a weighted fit was used, and the uncertainty in the parameterisation is 12.0 %, taken as the maximum magnitude of the 95 % confidence limit.

Comparison with literature measurements is only possible at room temperature, where we measure an average  $k_2 = (4.65 \pm 0.50) \times 10^{-12} \text{ cm}^3 \text{ molecule}^{-1} \text{ s}^{-1}$ , approximately 25 % slower than the only reported rate coefficient, by Platz et al.<sup>38</sup>, who found  $k_2 = (6.0 \pm 0.5) \times 10^{-12} \text{ cm}^3 \text{ molecule}^{-1} \text{ s}^{-1}$  at 295 K using pulsed radiolysis. There is no overlap of the two values' uncertainty ranges. Pulsed radiolysis can involve much higher radical concentrations, and hence fast radical-radical reactions, causing increased OH loss, may have affected the Platz et al. measurements.

Figure 7 shows what is possibly the onset of a negative temperature dependence region for  $k_2$ , at temperatures below approximately 340 K. Measurements of  $k_2$  at ~340 K and room temperature were both repeated to ensure the exhibited temperature dependence was unlikely to be the result of anomalous measurements. Low temperature studies have shown that a negative temperature dependence of the rate coefficient for OH + hydrocarbon reactions can occur below ~200 K. DME and acetone have both demonstrated this behaviour arising from the formation of a hydrogen-bonded pre-reaction complex forming, in which an H atom can subsequently quantum tunnel through the reaction barrier to form water.<sup>46</sup> Reaction 1 also shows slight evidence for negative temperature dependence around room temperature, but not so pronounced as for reaction 2. Bennett and Kerr<sup>13</sup> studied reaction 1 using a relative rate technique from 246 – 314 K finding a slight positive temperature dependence ( $E_a = 0.85 \pm 0.59 \text{ kJ mol}^{-1}$ ) although for diethyl ether and several other larger ethers, a negative temperature dependence was observed. Further studies of ethers at sub-ambient temperatures would be of mechanistic interest.

**Observation of OH recycling.** With OH recycling in the presence of oxygen for the MTBE system only occurring at higher temperatures, the formation mechanism was attributed to a route over a potential energy barrier high enough to inhibit OH formation in a system at lower thermal energy. Figure 8 shows a general schematic potential energy surface (PES) expected for ether oxidation, where the internal rearrangement of the RO<sub>2</sub> radical to the QOOH radical, and subsequent decomposition to OH and products is the most likely mechanism for OH recycling. The figure also includes a formally direct route to OH production by chemically activated decomposition of the RO<sub>2</sub> adduct. The energies of the RO<sub>2</sub>, QOOH, OH + products and the associated transition states are based on the values for DME.<sup>4</sup> For MTBE, the actual PES will be more complex as there are two different R radicals corresponding to initial abstraction from the CH<sub>3</sub> or t-C<sub>4</sub>H<sub>9</sub> groups. The  $k_b$  parameter (Figure 4) for the biexponential

fitting equation represents OH formed via this surface, and the  $k_c$  parameter represents the R radical not returning OH, which could be due to radical-radical reactions of the more stable  $RO_2$  radical, formation of  $HO_2$ , or at higher temperatures, decomposition of the R radical. In comparison to the DME/ $O_2$  system, the MTBE/ $O_2$  system shows three significant differences. Firstly, no chemically activated OH was observed in the MTBE/ $O_2$  system. Secondly, the yield of OH was significantly lower for MTBE/ $O_2$  than DME/ $O_2$  and thirdly, there was no evidence for interception of the QOOH when high concentrations of oxygen were used. We briefly outline the details of these observations and then link them to differences in the potential energy surfaces for DME/ $O_2$  and MTBE/ $O_2$ .

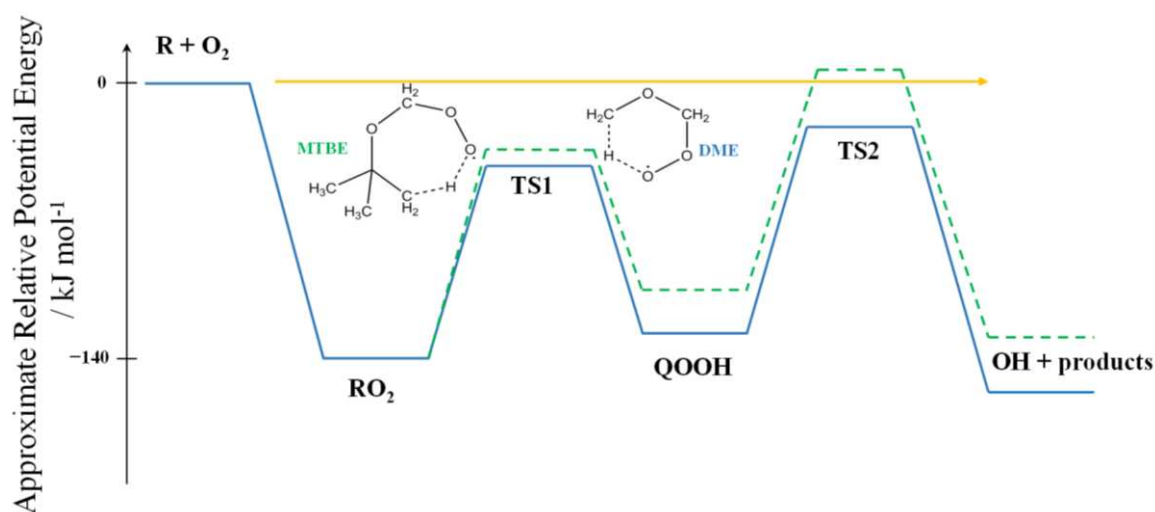


**Figure 8.** Generic potential energy surface for R radical low temperature combustion propagation for DME (blue solid line) and MTBE (green dashed line), including possible chemical activation route (gold line). Ring structures for the main MTBE abstraction route and DME are shown for the  $RO_2 \rightarrow QOOH$  transition state, and approximate relative potential energies are shown for the  $R + O_2$  and  $RO_2$  species, based on those for DME.

Chemical activation in low temperature combustion systems has been shown to be of importance at low pressures,<sup>4</sup> where the energised  $RO_2$  radical can “well-skip” to directly form the products from decomposition of QOOH before stabilization into the  $RO_2$  well (horizontal gold line in Figure 8). At pressures below 10 Torr of  $N_2$ , well-skipping has been observed in our previous studies on DME<sup>4</sup> and diethyl ether (DEE). Well-skipping is evidenced by the onset of biexponential decay traces at low  $[O_2]$ , where there is a linear relationship between removal of R ( $k_b + k_c$ ) and  $[O_2]$ , as the rate determining step in OH recycling is the  $R + O_2$  reaction to form chemically activated  $RO_2$ , which rapidly decomposes to OH + products. At 542 K, where no thermal decomposition of QOOH to OH occurs, (i.e. within the single-

exponential OH decay regime, see squares in Figure 6) no well-skipping/chemical activation could be positively identified for the MTBE system (9.1 – 10.7 Torr,  $[O_2] \approx (0.08 - 3) \times 10^{16}$  molecule  $cm^3$ ). Measurements were also taken at 578, 620 and 701 K, under low oxygen conditions ( $[O_2] \approx (0.05 - 2) \times 10^{16}$  molecule  $cm^3$ ) and low pressure conditions (9.3 – 10.2 Torr), and no significant dependence of the total removal rate of the R radical upon oxygen concentration was measured, again suggesting no well-skipping reactions.

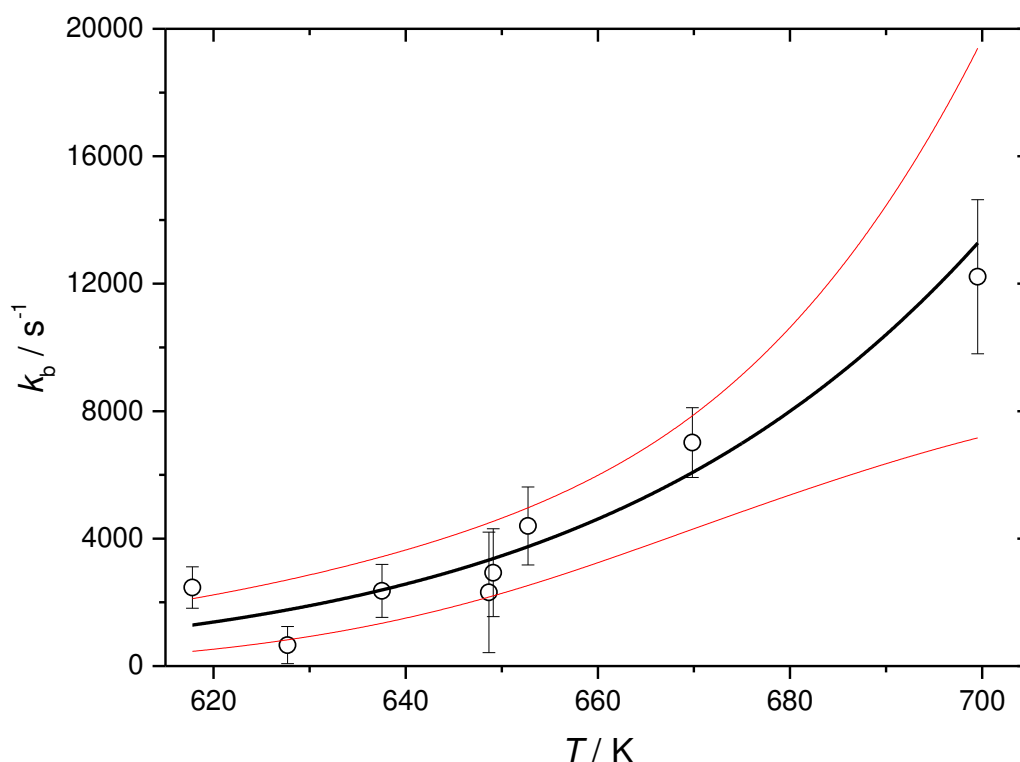


**Figure 9.** MTBE recycling rate coefficient,  $k_b$ , against temperature. Error bars are purely statistical at the  $2\sigma$  level. Red lines are the upper and lower bounds of the 95 % confidence limits. The data can be described by  $k_b(618-701 \text{ K}) = 6.05 \times 10^{11} \times \exp\left[\frac{-103000}{RT}\right] s^{-1}$ .

Figure 9 shows the positive temperature dependence of the recycling rate coefficient,  $k_b$ . Over the temperature range which the experiments could be conducted, the OH recycling rate coefficient exhibits an Arrhenius-like temperature dependence that is consistent with a process proceeding over a barrier. The data can be parameterised as  $k_b(618-701 \text{ K}) = 6.05 \times 10^{11} \times \exp\left[\frac{-103000}{RT}\right] s^{-1}$ , where the maximum value of the 95 % confidence limit uncertainty across the temperature studied was 64 %. This parameterisation yields an activation energy of

( $103 \pm 66$ )  $\text{kJ mol}^{-1}$ , which is comparable to the barrier heights expected based on DME.<sup>4</sup> Values for  $k_b$  presented in Figure 9 were obtained as a weighted average of all  $\text{O}_2$  concentration experiments ( $[\text{O}_2] \approx 10^{15} - 10^{18}$  molecule  $\text{cm}^{-3}$ ) for a given temperature, as no significant and reproducible dependence upon oxygen was seen (see Figure S3 in the Supporting Information).

The relationship between  $k_b$  and  $k_c$  for a given set of experimental conditions allows calculation of the percentage yield of OH using the following equation:

$$\text{OH yield \%} = \frac{k_b}{k_b + k_c} \times 100 \quad (\text{E4})$$

Here, the OH formation parameter,  $k_b$ , is expressed as a percentage of the total removal of the R radical ( $k_b + k_c$ ). An average yield of ( $36 \pm 5$ ) % (standard deviation was used to calculate the uncertainty in average yield for both molecules) was measured for MTBE across all temperatures, over the same range of  $[\text{O}_2]$  that was present in the  $k_b$  data presented above. Yields below approximately 620 K are not considered for MTBE, due to the low magnitude ( $< 1000 \text{ s}^{-1}$ ) of the temperature-dependent  $k_b$  parameters measured (Figure 9). At this order of magnitude,  $k_b$  is more likely to be perturbed by other slow chemistry, such as radical-radical reactions.

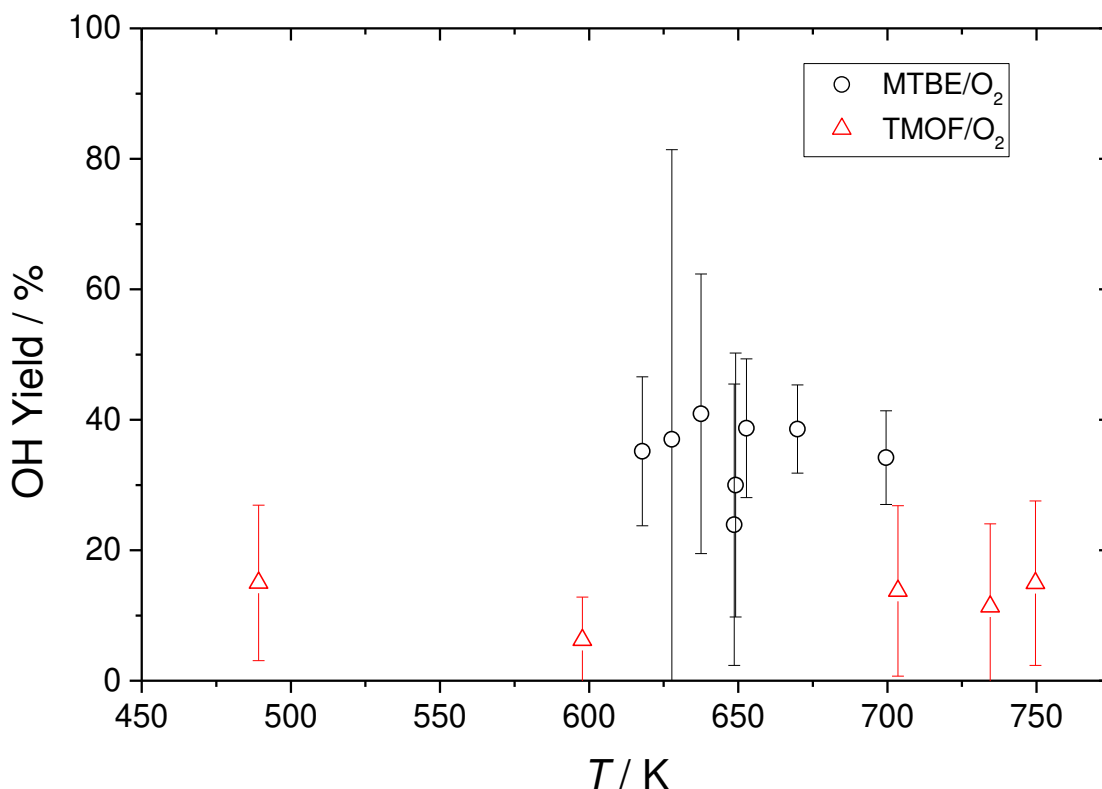


**Figure 10.** OH yields against temperature for MTBE/O<sub>2</sub> (black circles) and TMOF/O<sub>2</sub> (red triangles). Error bars are purely statistical at the 2 $\sigma$  level.

At high concentrations of oxygen ( $[O_2] > 10^{16}$  molecule cm<sup>-3</sup>) in DME and DEE systems, we see evidence for the interception of QOOH (to form O<sub>2</sub>QOOH) before decomposition to OH and co-products. However, at comparable concentrations of oxygen, there is no evidence for any change in mechanism in the MTBE/O<sub>2</sub> system; comparable concentrations of O<sub>2</sub> do not appear to intercept the MTBE-based QOOH radicals.

The above observations on the behaviours for the DME/O<sub>2</sub> and MTBE/O<sub>2</sub> systems can be related to differences in the PES for these two systems. The absence of chemically activated OH from the MTBE/O<sub>2</sub> system under conditions where chemically activated OH production is observed for DEE/O<sub>2</sub> and DME/O<sub>2</sub> suggests that TS1 and/or TS2 are much closer in energy to the R + O<sub>2</sub> entrance channel (or indeed above this value, as in Figure 8). Additionally, chemical activation in MTBE may be absent due to the seven-membered ring transition state between RO<sub>2</sub> and QOOH radicals being less entropically favourable compared to the six-membered ring formed in the DME system. Ogura et al.<sup>47</sup> calculated that the A factor for a seven-membered ring is only 12% of the six-membered ring equivalent. The larger size of MTBE may also increase the likelihood of collisional stabilisation into the potential energy surface wells,

inhibiting chemical activation, however chemical activation and significant well-skipping was observed for the comparably-sized DEE molecule.<sup>48</sup> Finally, the higher transition state barrier for  $\text{QOOH} \leftrightarrow \text{OH}$  in the MTBE system, as opposed to that for DME, could be harder to surmount as a result of the negative effects of entropy, and ring strain, required for formation of the 4,4-dimethyl-1,3-dioxolane species (Figure 11).

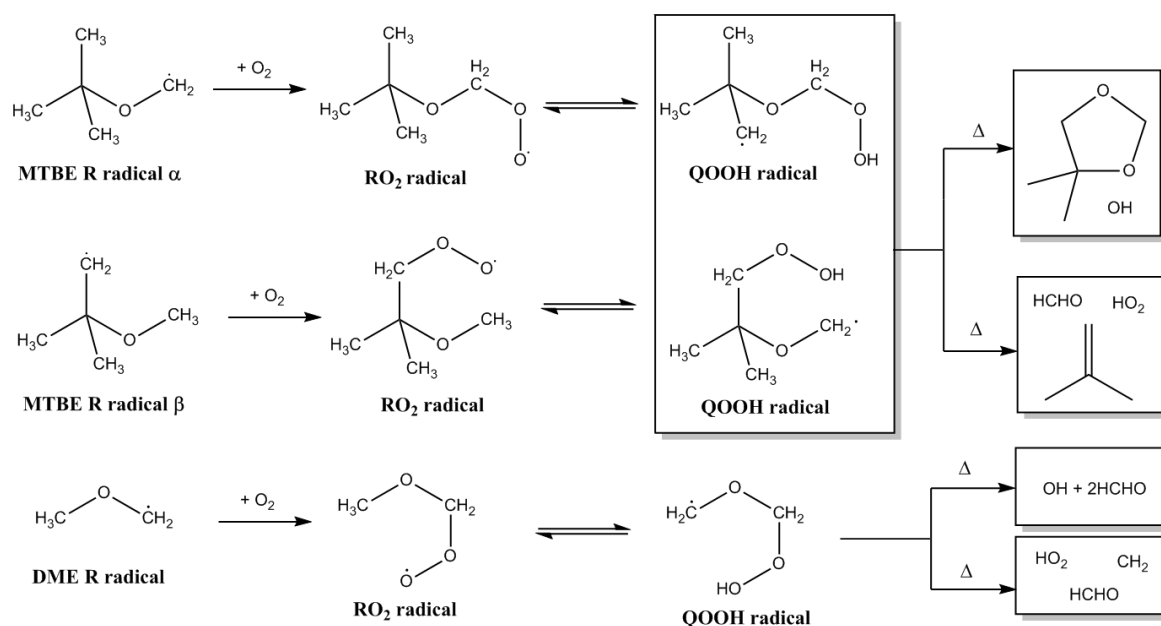


**Figure 11.** Comparison of R radical route to OH propagation, or  $\text{HO}_2$  formation, for MTBE and DME.

The OH yields observed from MTBE/ $\text{O}_2$  were relatively low (Figure 10) compared to similar ether biofuels, where yields closer to 100 % would be expected for a molecule such as DME.<sup>4</sup> Low yields suggest OH propagation is a minor channel of the low temperature oxidation system, and that another, non-OH producing reaction, dominates after the initial hydrogen abstraction from the ether. Decomposition of QOOH to  $\text{HO}_2$ ,  $\text{H}_2\text{CO}$  and isobutene<sup>15, 17, 49</sup> is the reaction reported as the major channel for the MTBE QOOH decomposition (Figure 11). The analogous decomposition for the QOOH radical for DME (Figure 11) would be to the less favourable  $\text{HO}_2$  + ethylene oxide channel ( $\text{HO}_2$  +  $\text{H}_2\text{CO}$  +  ${}^3\text{CH}_2$  is highly endothermic) and therefore this route does not dominate the DME system, resulting in higher OH yields.

The observation of a small, but still significant, OH yield contradicts some mechanistic studies on MTBE oxidation; for example, Brocard et al.<sup>15</sup> have no route to OH formation from the QOOH radicals formed following abstraction at the  $\alpha$  C-H of MTBE and only isobutene, methanol and formaldehyde are reported as products from a jet-stirred reactor (JSR) study at

726 K by Glaude et al.<sup>49</sup> However, Ciajolo et al.<sup>17</sup> in another JSR study, do report the production of yields of 4,4-dimethyl-1,3-dioxolane with identification by GC/MS. Direct comparison of yields with this work is not possible as it is not possible to account for the consumption of the dioxolane in the longer residence times of the JSR. However, the observations of this work and the earlier study of Ciajolo et al. suggest the need for further development of MTBE models to account for OH production from QOOH species.

Based on the dominant initial abstraction in OH + MTBE being from the  $\alpha$  hydrogen, the R radical in DME and MTBE both contain the C-O-CH<sub>2</sub>• group and hence the well depth of the RO<sub>2</sub> for both DME and MTBE should be very similar (Figure 8). In MTBE, the RO<sub>2</sub> → QOOH internal abstraction requires breaking a stronger primary C-H bond (not activated through close proximity to the ether oxygen as in DME), but for both MTBE and DME, a similar OO-H bond is formed. Therefore the transition state for the internal abstraction (TS1, Figure 8) and the QOOH radical will both be higher in energy. This would explain the lack of QOOH interception by O<sub>2</sub> observed for MTBE.

The higher the energy of the QOOH radical with respect to the RO<sub>2</sub> species, the harder it becomes to intercept QOOH with O<sub>2</sub>. By using the MESMER (Master Equation Solver for Multi Energy well Reactions) code,<sup>50</sup> a model based around the analogous potential energy surface for DEE (comparable to DME, but closer in molecular complexity to MTBE) can be adjusted to demonstrate similar results to those seen in this work. Calculations were based on conditions of 500 K and 25 Torr. OH yields arising from chemical activation for DEE can be inhibited by raising the barrier out to the OH product (TS2, Figure 8) by approximately 12 kJ mol<sup>-1</sup>. Similarly, the likelihood of chain-branching via the formation of O<sub>2</sub>QOOH can be lowered by reducing the well-depth of the QOOH species. Raising the height of QOOH relative to RO<sub>2</sub> by ~20 kJ mol<sup>-1</sup> can increase the RO<sub>2</sub>:QOOH concentration ratio by approximately a factor of ten, where ten times more O<sub>2</sub> would be required to form O<sub>2</sub>QOOH. While this MESMER modelling is only semi-quantitative, it shows the changes in the PES required to bring agreement with our experiment observations, see Figure 8.

Trimethyl orthoformate had a significantly lower average OH yield of (10 ± 3) % (Figure 10), and there is no clear route to HO<sub>2</sub> formation from TMOF's mechanism. As such, the mechanism behind the low TMOF yields is not understood. Additionally, there was no oxygen dependence seen with the rate of OH recycling for TMOF, and the  $k_b$  parameter returned was temperature-independent and of a very low order of magnitude (<400 s<sup>-1</sup>), which may be perturbed by secondary chemistry in the system, such as radical-radical reactions. It

was also noted that at ~690 K, OH fluorescence was present in the absence of H<sub>2</sub>O<sub>2</sub>, suggesting that TMOF was acting as a precursor to hydroperoxides at high temperature.

## Conclusion

The first temperature-dependent study of the rate coefficient for OH + TMOF has been carried out between 298 K and 744 K, where biexponential decays were observed above 489 K. A similar study between 298 K and 727 K was conducted for OH + MTBE, where the first observation of biexponential behaviour in the presence of O<sub>2</sub> was seen above 568 K. Evidence of OH recycling in both systems allowed OH yields to be measured.

A low average OH yield of (10 ± 3) % was measured for the TMOF system, but yields were higher for MTBE (36 ± 5 %). OH yields far below 100 % for MTBE were attributed to an alternative QOOH decomposition route, where the dominating channel was formation of HO<sub>2</sub>. Contrarily, the mechanism giving rise to such low yields for trimethyl orthoformate was not understood, and requires further investigation.

For both the MTBE and TMOF systems, future experimental studies will look at low temperature kinetics and direct measurements of the yields of HO<sub>2</sub> using a modified version of our high pressure OH detection system to allow for the detection of HO<sub>2</sub> via the FAGE technique. Furthermore, this system would allow the addition of up to ~10<sup>19</sup> molecule cm<sup>-3</sup> of oxygen to increase the likelihood of QOOH interception.

**Corresponding email address:** P.W.Seakins@leeds.ac.uk

## Supporting Information.

More details of data and analysis, including example TMOF bimolecular plot and decays,  $k_b$  vs O<sub>2</sub> behaviour for MTBE, OH yields, OH fluorescence from TMOF in the absence of H<sub>2</sub>O<sub>2</sub>, the full biexponential equation, and the MESMER input code.

## Acknowledgement

EPSRC grant number EP/L014912/1 for funding for DGP.

## References

1. International Energy Agency *Tracking Clean Energy Progress 2017*; IEA Publications, 2017.
2. Bansch, C.; Kiecherer, J.; Szöri, M.; Olzmann, M., Reaction of Dimethyl Ether with Hydroxyl Radicals: Kinetic Isotope Effect and Prereactive Complex Formation. *J. Phys. Chem. A* **2013**, *117*, 8343-8351.
3. Carr, S. A.; Still, T. J.; Blitz, M. A.; Eskola, A. J.; Pilling, M. J.; Seakins, P. W.; Shannon, R. J.; Wang, B.; Robertson, S. H., Experimental and Theoretical Study of the Kinetics and Mechanism of the Reaction of OH Radicals with Dimethyl Ether. *J. Phys. Chem. A* **2013**, *117*, 11142-54.
4. Eskola, A. J.; Carr, S. A.; Shannon, R. J.; Wang, B.; Blitz, M. A.; Pilling, M. J.; Seakins, P. W.; Robertson, S. H., Analysis of the Kinetics and Yields of OH Radical Production from the  $\text{CH}_3\text{OCH}_2 + \text{O}_2$  Reaction in the Temperature Range 195-650 K: An Experimental and Computational Study. *J. Phys. Chem. A* **2014**, *118*, 6773-88.
5. Hu, E. J.; Ku, J. F.; Yin, G. Y.; Li, C. C.; Lu, X.; Huang, Z. H., Laminar Flame Characteristics and Kinetic Modeling Study of Ethyl Tertiary Butyl Ether Compared with Methyl Tertiary Butyl Ether, Ethanol, iso-Octane, and Gasoline. *Energy Fuels* **2018**, *32*, 3935-3949.
6. Moshhammer, K.; Jasper, A. W.; Popolan-Vaida, D. M.; Lucassen, A.; Diévert, P.; Selim, H.; Eskola, A. J.; Taatjes, C. A.; Leone, S. R.; Sarathy, S. M., et al., Detection and Identification of the Keto-Hydroperoxide ( $\text{HOOCH}_2\text{OCHO}$ ) and Other Intermediates during Low-Temperature Oxidation of Dimethyl Ether. *J. Phys. Chem. A* **2015**, *119*, 7361-7374.
7. Zhang, X.; Oyedun, A.; Kumar, A.; Oestreich, D.; Arnold, U.; Sauer, J., An Optimized Process Design for Oxymethylene Ether Production from Woody-Biomass-Derived Syngas. *Biomass Bioenergy* **2016**, *90*, 7-14.
8. Ford; Ford Leads Project to Develop Near Zero Particulate Emission Diesel Cars that Could Run on Converted  $\text{CO}_2$ . <https://media.ford.com/> (accessed 10/05/2018).
9. Volvo *The Volvo Group Annual and Sustainability Report*; Goteborg, Sweden, 2015.
10. Boot, M. D.; Tian, M.; Hensen, E. J. M.; Mani Sarathy, S., Impact of Fuel Molecular Structure on Auto-Ignition Behavior – Design Rules for Future High Performance Gasolines. *Prog. Energy Combust. Sci.* **2017**, *60*, 1-25.
11. Tsolakis, A.; Megaritis, A.; Yap, D., Application of Exhaust Gas Fuel Reforming in Diesel and Homogeneous Charge Compression Ignition (HCCI) Engines Fuelled with Biofuels. *Energy* **2008**, *33*, 462-470.
12. Arif, M.; Dellinger, B.; Taylor, P. H., Rate Coefficients of Hydroxyl Radical Reaction with Dimethyl Ether and Methyl tert-Butyl Ether over an Extended Temperature Range. *J. Phys. Chem. A* **1997**, *101*, 2436-2441.

13. Bennett, P. J.; Kerr, J. A., Kinetics of the Reactions of Hydroxyl Radicals with Aliphatic Ethers Studied under Simulated Atmospheric Conditions: Temperature Dependences of the Rate Coefficients. *J. Atmos. Chem.* **1990**, *10*, 27-38.
14. Bonard, A.; Daële, V.; Delfau, J.-L.; Vovelle, C., Kinetics of OH Radical Reactions with Methane in the Temperature Range 295–660 K and with Dimethyl Ether and Methyl-tert-butyl Ether in the Temperature Range 295–618 K. *J. Phys. Chem. A* **2002**, *106*, 4384-4389.
15. Brocard, J. C.; Baronnet, F.; O'Neal, H. E., Chemical Kinetics of the Oxidation of Methyl tert-Butyl Ether (MTBE). *Combust. Flame* **1983**, *52*, 25-35.
16. Chiung-Ju, C. Experiment, Thermodynamic Properties and Modeling on Combustion of Methyl tert-Butyl Ether: Isobutane and Isobutene and Thermodynamic Properties of Chloro Alkanes and Alkenes. New Jersey's Science & Technology University, 2000.
17. Ciajolo, A., Low-Temperature Oxidation of MTBE in a High-Pressure Jet-Stirred Flow Reactor. *Combust. Sci. Technol.* **1997**, *123*, 49-61.
18. Picquet, B.; Heroux, S.; Chebbi, A.; Doussin, J. F.; Durand-Jolibois, R.; Monod, A.; Loirat, H.; Carlier, P., Kinetics of the Reactions of OH Radicals with Some Oxygenated Volatile Organic Compounds under Simulated Atmospheric Conditions. *Int. J. Chem. Kinet.* **1998**, *30*, 839-847.
19. Smith, D. F.; Kleindienst, T. E.; Hudgens, E. E.; McIver, C. D.; Bufalini, J. J., The Photooxidation of Methyl Tertiary Butyl Ether. *Int. J. Chem. Kinet.* **1991**, *23*, 907-924.
20. Teton, S.; Mellouki, A.; Bras, G. L.; Sidebottom, H., Rate Constants for Reactions of OH Radicals with a Series of Asymmetrical Ethers and tert-Butyl Alcohol. *Int. J. Chem. Kinet.* **1996**, *28*, 291-297.
21. Wallington, T. J.; Andino, J. M.; Skewes, L. M.; Siegl, W. O.; Japar, S. M., Kinetics of the Reaction of OH Radicals with a Series of Ethers under Simulated Atmospheric Conditions at 295 K. *Int. J. Chem. Kinet.* **1989**, *21*, 993-1001.
22. Wallington, T. J.; Dagaut, P.; Liu, R.; Kurylo, M. J., Gas-Phase Reactions of Hydroxyl Radicals with the Fuel Additives Methyl tert-Butyl Ether and tert-Butyl Alcohol over the Temperature Range 240-440 K. *Environ. Sci. Technol.* **1988**, *22*, 842-4.
23. Erickson, J. G., Alkyl Orthoformates. *J. Org. Chem.* **1955**, *20*, 1573-1576.
24. M. Adams, J.; E. Clement, D.; H. Graham, S., Synthesis of Methyl-t-Butyl Ether from Methanol and Isobutene Using a Clay Catalyst. *Clay. Clay Miner.* **1982**, *30*, 129-134.
25. Prakash, G. K. S.; Smart, M. C.; Olah, G. A.; Narayanan, S. R.; Chun, W.; Surampudi, S.; Halpert, G., Performance of Dimethoxymethane and Trimethoxymethane in Liquid-Feed Direct Oxidation Fuel Cells. *J. Power Sources* **2007**, *173*, 102-109.
26. Wang, J. T.; Lin, W. F.; Weber, M.; Wasmus, S.; Savinell, R. F., Trimethoxymethane as an Alternative Fuel for a Direct Oxidation PBI Polymer Electrolyte Fuel Cell. *Electrochim. Acta* **1998**, *43*, 3821-3828.

27. Walker, R. W.; Morley, C., Chapter 1 Basic Chemistry of Combustion. In *Comprehensive Chemical Kinetics*, Pilling, M. J., Ed. Elsevier: Amsterdam, 1997; Vol. 35, pp 1-124.
28. Pilling, M. J.; Robertson, S. H.; Seakins, P. W., Elementary Radical Reactions and Autoignition. *J. Chem. Soc., Faraday Trans.* **1995**, *91*, 4179-4188.
29. Robertson, S. H.; Seakins, P. W.; Pilling, M. J., Low-Temperature Combustion and Auto-Ignition. In *Comprehensive Chemical Kinetics*, Pilling, M. J., Ed. Elsevier: Amsterdam, 1997; Vol. 35.
30. Jenkin, M. E.; Hayman, G. D.; Wallington, T. J.; Hurley, M. D.; Ball, J. C.; Nielsen, O. J.; Ellermann, T., Kinetic and Mechanistic Study of the Self-Reaction of Methoxymethylperoxy Radicals at Room Temperature. *J. Phys. Chem.* **1993**, *97*, 11712-11723.
31. Westbrook, C. K., Chemical Kinetics of Hydrocarbon Ignition in Practical Combustion Systems. *Proc. Combust. Inst.* **2000**, *28*, 1563-1577.
32. Zádor, J.; Taatjes, C. A.; Fernandes, R. X., Kinetics of Elementary Reactions in Low-Temperature Autoignition Chemistry. *Prog. Energy Combust. Sci.* **2011**, *37*, 371-421.
33. Japar, S. M.; Wallington, T. J.; Richert, J. F. O.; Ball, J. C., The Atmospheric Chemistry of Oxygenated Fuel Additives: t-Butyl Alcohol, Dimethyl Ether, and Methyl t-Butyl Ether. *Int. J. Chem. Kinet.* **1990**, *22*, 1257-1269.
34. Tuazon, E. C.; Carter, W. P. L.; Aschmann, S. M.; Atkinson, R., Products of the Gas-Phase Reaction of Methyl tert-Butyl Ether with the OH Radical in the Presence of NO<sub>x</sub>. *Int. J. Chem. Kinet.* **1991**, *23*, 1003-1015.
35. Iuga, C.; Osnaya-Soto, L.; Ortiz, E.; Vivier-Bunge, A., Atmospheric Oxidation of Methyl and Ethyl tert-Butyl Ethers Initiated by Hydroxyl Radicals. A Quantum Chemistry Study. *Fuel* **2015**, *159*, 269-279.
36. Zavala-Oseguera, C.; Alvarez-Idaboy, J. R.; Merino, G.; Galano, A., OH Radical Gas Phase Reactions with Aliphatic Ethers: A Variational Transition State Theory Study. *J. Phys. Chem. A* **2009**, *113*, 13913-13920.
37. Atadinc, F.; Selcuki, C.; Sari, L.; Aviyente, V., Theoretical Study of Hydrogen Abstraction from Dimethyl Ether and Methyl tert-Butyl Ether by Hydroxyl Radical. *Phys. Chem. Chem. Phys.* **2002**, *4*, 1797-1806.
38. Platz, J.; Sehested, J.; Nielsen, O. J.; Wallington, T. J., Atmospheric Chemistry of Trimethoxymethane, (CH<sub>3</sub>O)<sub>3</sub>CH; Laboratory Studies. *J. Phys. Chem. A* **1999**, *103*, 2632-2640.
39. Porter, E.; Wenger, J.; Treacy, J.; Sidebottom, H.; Mellouki, A.; Téton, S.; LeBras, G., Kinetic Studies on the Reactions of Hydroxyl Radicals with Diethers and Hydroxyethers. *J. Atmos. Chem. A* **1997**, *101*, 5770-5775.
40. Wallington, T. J.; Hurley, M. D.; Ball, J. C.; Straccia, A. M.; Platz, J.; Christensen, L. K.; Sehested, J.; Nielsen, O. J., Atmospheric Chemistry of Dimethoxymethane (CH<sub>3</sub>OCH<sub>2</sub>OCH<sub>3</sub>):

Kinetics and Mechanism of its Reaction with OH Radicals and Fate of the Alkoxy Radicals  $\text{CH}_3\text{OCHO}(\bullet)\text{OCH}_3$  and  $\text{CH}_3\text{OCH}_2\text{OCH}_2\text{O}(\bullet)$ . *J. Phys. Chem. A* **1997**, *101*, 5302-5308.

41. Onel, L.; Blitz, M. A.; Breen, J.; Rickard, A. R.; Seakins, P. W., Branching Ratios for the Reactions of OH with Ethanol Amines Used in Carbon Capture and the Potential Impact on Carcinogen Formation in the Emission Plume from a Carbon Capture Plant. *Phys. Chem. Chem. Phys.* **2015**, *17*, 25342-25353.
42. Onel, L.; Blitz, M. A.; Seakins, P. W., Direct Determination of the Rate Coefficient for the Reaction of OH Radicals with Monoethanol Amine (MEA) from 296 to 510 K. *J. Phys. Chem.* **2012**, *3*, 853-856.
43. Orkin, V. L.; Villenave, E.; Huie, R. E.; Kurylo, M. J., Atmospheric Lifetimes and Global Warming Potentials of Hydrofluoroethers: Reactivity toward OH, UV Spectra, and IR Absorption Cross Sections. *J. Phys. Chem. A* **1999**, *103*, 9770-9779.
44. Tranter, R. S.; Walker, R. W., Rate Constants for the Reactions of H Atoms and OH Radicals with Ethers at 753 K. *Phys. Chem. Chem. Phys.* **2001**, *3*, 4722-4732.
45. Yasunaga, K.; Simmie, J. M.; Curran, H. J.; Koike, T.; Takahashi, O.; Kuraguchi, Y.; Hidaka, Y., Detailed Chemical Kinetic Mechanisms of Ethyl Methyl, Methyl tert-Butyl and Ethyl tert-Butyl Ethers: The Importance of Uni-Molecular Elimination Reactions. *Combust. Flame* **2011**, *158*, 1032-1036.
46. Shannon, R. J.; Caravan, R. L.; Blitz, M. A.; Heard, D. E., A Combined Experimental and Theoretical Study of Reactions Between the Hydroxyl Radical and Oxygenated Hydrocarbons Relevant to Astrochemical Environments. *Phys. Chem. Chem. Phys.* **2014**, *16*, 3466-3478.
47. Ogura, T.; Miyoshi, A.; Koshi, M., Rate Coefficients of H-Atom Abstraction from Ethers and Isomerization of Alkoxyalkylperoxy Radicals. *Phys. Chem. Chem. Phys.* **2007**, *9*, 5133-5142.
48. Potter, D. G.; Blitz, M. A.; Medeiros, D. J.; Wiseman, S.; Seakins, P. W., Direct Observations of the Low Temperature Oxidation of Diethyl Ether. *Manuscript in Preparation* **2018**.
49. Glaude, P. A.; Battin-Leclerc, F.; Judenherc, B.; Warth, V.; Fournet, R.; Côme, G. M.; Scacchi, G.; Dagaut, P.; Cathonnet, M., Experimental and modeling study of the gas-phase oxidation of methyl and ethyl tertiary butyl ethers. *Combust. Flame* **2000**, *121*, 345-355.
50. Glowacki, D. R.; Liang, C. H.; Morley, C.; Pilling, M. J.; Robertson, S. H., MESMER: An Open-Source Master Equation Solver for Multi-Energy Well Reactions. *J. Phys. Chem. A* **2012**, *116*, 9545-9560.